Water Science and Engineering, **Jun. 2008, Vol. 1, No. 2, 88–101**
ISSN 1674–2370, *http://kkb.hhu.edu.cn*, e-mail: *wse@hhu.edu.cn*

Nonlinear simulation of arch dam cracking with mixed finite element method

Ren Hao*, Li Tongchun, Chen Huifang, Zhao Lanhao

College of Water Conservancy and Hydropower Engineering, Hohai University, Nanjing 210098, P. R. China

Abstract: This paper proposes a new, simple and efficient method for nonlinear simulation of arch dam cracking from the construction period to the operation period, which takes into account the arch dam construction process and temperature loads. In the calculation mesh, the contact surface of pair nodes is located at places on the arch dam where cracking is possible. A new effective iterative method, the mixed finite element method for friction-contact problems, is improved and used for nonlinear simulation of the cracking process. The forces acting on the structure are divided into two parts: external forces and contact forces. The displacement of the structure is chosen as the basic variable and the nodal contact force in the possible contact region of the local coordinate system is chosen as the iterative variable, so that the nonlinear iterative process is only limited within the possible contact surface and is much more economical. This method was used to simulate the cracking process of the Shuanghe Arch Dam in Southwest China. In order to prove the validity and accuracy of this method and to study the effect of thermal stress on arch dam cracking, three schemes were designed for calculation. Numerical results agree with actual measured data, proving that it is feasible to use this method to simulate the entire process of nonlinear arch dam cracking.

Key words: *mixed finite element method*; *contact pair nodes*; *crack of arch dam*; *simulation*; *thermal stress*

DOI: 10.3882/j. issn. 1674-2370.2008.02.009

1 Introduction

Thermal stress is one of the main causes of cracks in arch dams. Due to long calculation terms and massive calculation steps, it is relatively difficult to consider the nonlinear cracking process from the construction period to the operation period in simulation of temperature fields and stress fields with the finite element method (FEM). Scholars have used joint elements to simulate temperature cracks in arch dams (Zhang et al. 2004; Yang 2003) and solved the crack contact problem with the penalty method (Simo et al. 1985; Wang et al. 1998) and the Lagrange multiplier method (Kikuhci 1982; Peric and Owen 1992; Lei et al 1994; Shao et al. 1999). The traditional methods usually consider the total degrees of freedom (DOF) of the entire system to be the iterative variables, resulting in a large computation load. Decomposition of numerous stiffness matrices is required at every time step throughout the process of simulation of arch dam cracks, leading to the substantial computational complexity and lowering the efficiency of calculation. Because the contact problem is a local nonlinear problem, the contact nonlinearity only comes from the possible contact region, which is a small part of the whole model. A new and highly efficient iterative method—the mixed finite

This work was supported by the National Nature Science Foundation of China (Grant No. 90510017).
*Corresponding author (e-mail: *renhaohhu@163.com*)
Received Apr. 8, 2008; accepted May 8, 2008

element method (Francavilla and Zienkiewicz 1975; Haug and Saxce 1980; Zhao et al. 2006, 2007), a node-to-node contact algorithm for contact problems with friction and initial gaps, has been improved in this study. Because of the local nonlinearity of this problem, only the nodal contact forces in the potential contact region are chosen as the iterative variables in the local coordinate system of the proposed method. Therefore, the nonlinear iterative process is only limited within the possible contact surfaces and can be very economical. In this way, the sophisticated contact nonlinearity is demonstrated by the variety of contact forces, which are determined by the external load and the contact state, i.e., stick, slip or separation. The iterative process, both for contact forces and the contact state, is carried out during simulation. Some parameters for other methods that are difficult to determine or sensitive to the results, such as the normal and tangential stiffness, penalty factors, etc. are not required in this algorithm. In this study, the method was improved and used to simulate the cracking process of an arch dam from construction through operation. The accuracy and feasibility of this method are proved through comparison of the results of three calculation schemes with actual data.

2 Calculation method

2.1 Unsteady temperature field analysis

The temperature of concrete changes during the construction of an arch dam due to the effect of hydration heat of cement. This problem can be expressed as a heat conduction problem with internal heat sources in the area R. The unsteady temperature field $T(x, y, z, \tau)$ is written as

$$\frac{\partial T}{\partial \tau} = a\left(\frac{\partial^2 T}{\partial x^2} + \frac{\partial^2 T}{\partial y^2} + \frac{\partial^2 T}{\partial z^2}\right) + \frac{\partial \theta}{\partial \tau} \tag{1}$$

where a is the thermal diffusivity of concrete, and θ is the adiabatic temperature rise of concrete. The boundary value conditions are (a) the initial condition $\tau = 0$, $T = T_a(x, y, z)$; (b) the known boundary $T = T_b$; (c) the heat dissipation boundary $\lambda \frac{\partial T}{\partial n} + \beta(T - T_a) = 0$; and (d) the adiabatic boundary $\frac{\partial T}{\partial n} = 0$, in which, T_a and T_b are the given temperature boundaries, λ is the thermal conductivity of concrete, n is the normal direction to the surface, and β is the film coefficient of heat transfer of concrete.

In the simulation analysis of the temperature field, the layer pouring and placing temperature, construction intermission and heat dissipation boundary condition need to be simulated. Setting the initial temperature value of the element of the pouring layer to be equal to the placing temperature can simulate the placing temperature. The construction intermission can be simulated by adjusting the calculation time step. The stiffness matrix of the FEM equation is re-formed continuously according to the construction process in order to simulate the shape-changing of the dam. However, because of the complex structure, the heat

dissipation boundary condition constantly changes with the layer pouring and its simulation is relatively difficult. Therefore, an automatic heat dissipation boundary method based on the characteristics of the FEM is presented in this paper. A 3D eight-node isoparametric element has six surfaces. Assuming that there are N elements, $6\times N$ surfaces can be obtained by separating all the elements. All surfaces can be divided into two types. A surface of the first type is connected with only one element, belongs to the boundary surface of the calculation area, and isn't overlapped by any other surface of the same type; a surface of the second type is the internal surface, which belongs to two elements simultaneously, and is certainly overlapped by another surface. The heat dissipation boundary surfaces are of the first type, and they are easily to be identified with a computer program.

2.2 Formulations of mixed finite element method

The contact problem is a fairly complex mechanical phenomenon in practice. When it is described as a mechanical model, three principles must always be satisfied to obtain the correct solution: (1) the impenetration condition, in which no material particle is allowed to penetrate the surface of the opposite body; (2) the normal traction condition, in which the normal traction between two bodies is compressive or zero; and (3) the frictional condition, which represents the relationship between the normal traction and tangential traction, described by the Mohr-Coulomb friction law. The contact conditions of the contact model shown in Figure 1 are summarized in Table 1.

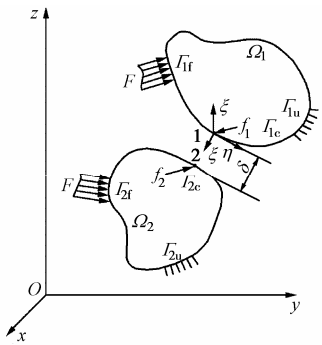

Figure 1 Mechanical model for contact problems

Table 1 Contact conditions for contact problems with friction and initial gaps

Contact status	Equality constraint	Inequality constraint
Separation	$\boldsymbol{f}_1 = \boldsymbol{f}_2 = 0$	$\delta > 0$
Stick	$\delta = 0$, $\boldsymbol{f}_1 = -\boldsymbol{f}_2$	$f_\xi < \sigma_t A$, $\sqrt{f_\eta^2 + f_\zeta^2} < -\mu f_\xi + Ac$
Slip	$\delta = 0$, $\sqrt{f_\eta^2 + f_\zeta^2} = -\mu f_\xi + Ac$	$f_\xi < \sigma_t A$

In Table 1, A is the tributary area of node 1 or 2; μ is the friction coefficient; c is the cohesive strength; σ_t is the specified tensile strength; δ is the gap between node 1 and node 2 measured in the normal direction, $\delta = (\boldsymbol{u}_1 - \boldsymbol{u}_2)\cdot\boldsymbol{\xi} + \delta_0$, in which $\boldsymbol{\xi}$ is the normal direction to the contact region, δ_0 is the initial normal gap between node 1 and node 2, and $\boldsymbol{u}_1$ and $\boldsymbol{u}_2$ are the displacements of node 1 and node 2; f_ξ, f_η and f_ζ are components of contact force $\boldsymbol{f}$ in local coordinates ξ, η and ζ, respectively; and $\boldsymbol{f}_1$ and $\boldsymbol{f}_2$ are contact forces on Γ_{1c}.

Assuming that the analysis of the *n*th step (at time *t*) is finished, the incremental static equilibrium equation for the *n*+1th step (at time $t+\Delta t$) is as follows:

$$\boldsymbol{K}\Delta\boldsymbol{u}_n = (\boldsymbol{F}_{n+1} + \boldsymbol{f}_n - \int \boldsymbol{B}^{\mathrm{T}}\boldsymbol{\sigma}_n \mathrm{d}\Omega) + \Delta\boldsymbol{f}_n \tag{2}$$

where $\boldsymbol{K}$ is the global stiffness matrix, $\Delta\boldsymbol{u}_n$ is the vector of displacement increment at time *t*, $\boldsymbol{F}_{n+1}$ is the vector of the total external load at time $t+\Delta t$, $\boldsymbol{f}_n$ is the vector of the total contact force at time *t*, $\boldsymbol{B}$ is the strain-displacement matrix, $\boldsymbol{\sigma}_n$ is the Cauchy stress tensor at time *t*, and $\Delta\boldsymbol{f}_n$ is the vector of incremental contact force at time *t*. Clearly, the first term on the right-hand side of Eq. (2), i.e., the content in the bracket, stands for the external load increment of the current time step, since the contribution of $\boldsymbol{f}_n$ to the system is already included in $\boldsymbol{\sigma}_n$.

If a typical decomposition of global stiffness matrix $\boldsymbol{K}$ is performed for only one time at the beginning of the analysis, Eq. (2) can be alternatively written as

$$\Delta\boldsymbol{u}_n = \boldsymbol{K}^{-1}(\boldsymbol{F}_{n+1} + \boldsymbol{f}_n - \int \boldsymbol{B}^{T}\boldsymbol{\sigma}_n \mathrm{d}\Omega) + \boldsymbol{K}^{-1}\Delta\boldsymbol{f}_n \tag{3}$$

where $\Delta\bar{\boldsymbol{u}}_n$ is defined as

$$\Delta\bar{\boldsymbol{u}}_n = \boldsymbol{K}^{-1}(\boldsymbol{F}_{n+1} + \boldsymbol{f}_n - \int \boldsymbol{B}^{T}\boldsymbol{\sigma}_n \mathrm{d}\Omega) \tag{4}$$

Introducing matrix $\boldsymbol{C}$ into the equation above leads to Eq. (5):

$$\Delta\boldsymbol{u}_n = \Delta\bar{\boldsymbol{u}}_n + \boldsymbol{C}\Delta\boldsymbol{f}_n \tag{5}$$

where matrix $\boldsymbol{C}$ is the flexibility matrix, which is defined at the possible contact boundary Γ_{1c}. An arbitrary component c_{ij} in matrix $\boldsymbol{C}$ represents the flexibility coefficient corresponding to the displacement at freedom *i* due to a unit force at freedom *j*. Here *i* and *j* are only limited within the freedom of the region where contact is likely to take place.

It is important to note that Eq. (4), Eq. (5) and the following equations in this section are only applied to the DOF of the possible contact surface, not the DOF of the whole system.

Applying Eq. (5) to nodes 1 and 2 of a given node pair yields

$$\Delta\boldsymbol{u}_{1n} = \Delta\bar{\boldsymbol{u}}_{1n} + \boldsymbol{C}_1\,\Delta\boldsymbol{f}_{1n} \tag{6}$$

$$\Delta\boldsymbol{u}_{2n} = \Delta\bar{\boldsymbol{u}}_{2n} + \boldsymbol{C}_2\Delta\boldsymbol{f}_{2n} \tag{7}$$

According to Newton's third law, $\Delta\boldsymbol{f}_{1n} = -\Delta\boldsymbol{f}_{2n} = \Delta\boldsymbol{f}_n$. Moreover, incorporating flexibility matrices $\boldsymbol{C}_1$ and $\boldsymbol{C}_2$ into $\boldsymbol{C} = \boldsymbol{C}_1 + \boldsymbol{C}_2$, and subtracting Eq. (7) from Eq. (6), we obtain

$$\boldsymbol{C}\Delta\boldsymbol{f}_n = (\Delta\boldsymbol{u}_{1n} - \Delta\boldsymbol{u}_{2n}) - (\Delta\bar{\boldsymbol{u}}_{1n} - \Delta\bar{\boldsymbol{u}}_{2n}) \tag{8}$$

Eq. (8) is the finite element compliance equation of the mixed finite element method for the static contact problems with friction and initial gaps. In this equation, the second term $(\Delta\bar{\boldsymbol{u}}_{1n} - \Delta\bar{\boldsymbol{u}}_{2n})$ on the right-hand side stands for the difference between the incremental displacements of node 1 and 2 only due to the external load increment, as can easily be seen from Eq. (4). Therefore, it has nothing to do with the current contact state and can be obtained by back-substitution directly. The first term $(\Delta\boldsymbol{u}_{1n} - \Delta\boldsymbol{u}_{2n})$ on the right-hand side denotes the difference between the incremental displacements induced by both the external load increment and the contact force increment. From this point of view, we can see that both the right-hand

and the left-hand sides of the above equation are associated with the contact state. An iterative method taking into account different contact states is necessary to solve Eq. (8). Further details of the iteration process will be given below.

2.3 Iteration process

Considering the contact conditions and finite element formulations described in section 2.2, the algorithm for static contact problems can be summarized as follows:

(1) The global stiffness matrix $\boldsymbol{K}$ is assembled from the element stiffness matrix $\boldsymbol{k}$. Each component of the flexibility matrix $\boldsymbol{C}$ that might be used during the iteration is obtained through the unit force algorithm by decomposition of matrix $\boldsymbol{K}$.

(2) When the analysis of the nth step is finished, one comes to the next time step, n+1. The contact forces and contact state of the last step are assumed to be the initial input condition. The value of $\Delta\overline{\boldsymbol{u}}_n$ can be determined simply by back-substitution of Eq. (4) with the known external force increment.

(3) After the ith iteration is finished, one comes to the next (i+1) iteration both for the contact state and contact forces. The contact state and contact forces at the ith iteration are transmitted to the current iteration step. Different treatments will be carried out according to different contact states as follows:

a. The current contact state is separated. The value of gaps between two bodies is calculated with the equation $\delta_{n+1}^{i+1} = \delta_{n+1}^{i} + (\Delta\boldsymbol{u}_{1n}^{i} - \Delta\boldsymbol{u}_{2n}^{i}) \cdot \boldsymbol{\xi}$, where $\Delta\boldsymbol{u}_{1n}^{i}$ and $\Delta\boldsymbol{u}_{2n}^{i}$ come from the results of the last iteration step. Here and throughout this paper, the superscript i denotes the iteration step while the subscript n stands for the loading increment step. A value of δ_{n+1}^{i+1} less than or equal to zero implies that the bodies are brought into contact now and produce an overlap. Therefore, the contact state is changed from separation to stick directly. Moreover, in the case when δ_{n+1}^{i+1} is less than zero, we set δ_{n+1}^{i+1} to zero to satisfy the impenetration condition described in section 2.

b. The current contact state is slip or stick. The normal stress component $(\sigma_n^{i+1})_{\xi}$ is obtained from the equation $(\sigma_n^{i+1})_{\xi} = \boldsymbol{\sigma}_n^{i+1} \cdot \boldsymbol{\xi}$. If $(\sigma_n^{i+1})_{\xi}$ is larger than σ_{t}^{i}, separation will occur according to the normal traction condition. Therefore, the current contact state is changed to separation, and $\boldsymbol{f}_{n+1}^{i+1} = 0$ and σ_n^{i+1}=0.

c. The current contact state is slip or stick after a. and b. The total tangential contact forces are obtained first, then the Mohr-Coulomb friction law is employed to determine whether slipping will occur or not according to the frictional condition. The contact state is changed from stick to slip if there is slipping taking place. At last, three freedoms of each node pair in the stick state and the normal freedom of each node pair in the slip state are marked to determine the size of the flexibility matrix in the current iteration step.

(4) A convergence check is performed for the contact state. The sign *icsta* is used to indicate whether the contact state iteration converges or not: 0 if the iteration isn't convergent and 1 if the iteration is convergent. If the contact state of all the pair nodes is identical to the

state in last iteration step, *icsta* is set to 1 and we go to step (6).

(5) The flexibility matrix $\boldsymbol{C}$ is assembled and decomposed. Only the freedoms marked in step (3) are included.

(6) The finite element compliance Eq. (8) is solved by back-substitution to obtain the iterative increment of contact forces $\Delta \boldsymbol{f}^i$

$$\Delta \boldsymbol{f}^i = \boldsymbol{C}^{-1}(\Delta \boldsymbol{u}_{1n}^i - \Delta \boldsymbol{u}_{2n}^i) - (\Delta \bar{\boldsymbol{u}}_{1n} - \Delta \bar{\boldsymbol{u}}_{2n}) \tag{9}$$

Then the contact force increment for the *n*th loading step after the current iteration is obtained

$$\Delta f_n^i = f_{n+1}^i + \Delta f^i - f_n \tag{10}$$

(7) A convergence check for contact forces is performed. The contact forces convergence criterion employed here is

$$\left| \boldsymbol{f}_{n+1}^{i+1} - \boldsymbol{f}_{n+1}^{i} \right| < \varepsilon \tag{11}$$

where ε is a predefined tolerable limit. A sign used to indicate whether the contact force iteration is convergent or not, *icfor*, is set to 1 if Eq. (11) is satisfied, and 0 in other conditions. If convergence for both the contact state and contact forces are achieved, i.e., *icsta* = 1 and *icfor* = 1, we proceed to step (9). Otherwise, we continue.

(8) The new iterative increment of displacement $\Delta \boldsymbol{u}_n^{i+1}$ is obtained according to equilibrium Eq. (3)

$$\Delta \boldsymbol{u}_n^{i+1} = \boldsymbol{K}^{-1}(\boldsymbol{F}_{n+1} + \boldsymbol{f}_n - \int \boldsymbol{B}^{\mathrm{T}} \boldsymbol{\sigma}_n d\Omega) + \boldsymbol{K}^{-1} \Delta \boldsymbol{f}_n^i \tag{12}$$

Then we turn to step (3) to continue the next iteration for the contact state and contact forces.

(9) The actual contact forces increment $\Delta \boldsymbol{f}_n$ of the *n*th loading step in equilibrium Eq. (2) is used to solve the actual displacement increment. Step (2) is repeated until all the time steps are finished.

3 Simulation analysis of nonlinear cracking process of Shuanghe Arch Dam

3.1 Description of Shuanghe Arch Dam

The Shuanghe Arch Dam is located in the estuary of the Shuanghe River, which is a branch of the Guixi River in the town of Xinming in Dianjiang County, Sichuan Province, China. The characteristics of the Shuanghe Arch Dam are as follows: the dam is a hyperbolic concrete arch dam with a masonry structure, a maximum height of 64.56 m, a crest elevation of 552.26 m, a normal high water level elevation of 548.60 m, a thickness of 2.5 m at the crest and 15 m at the bottom, an inner chord length of 137 m at the crest and 15 m at the bottom, a central angle of 84° at the crest and 30° at the bottom, a span-height ratio of 2.12 and a thick-height ratio of 0.23. There is no sluice gate on the crest spillway and an overflow weir is set in the middle of the dam crest. The weir crest elevation is 548.60 m and the spillway length

is 32.5 m.

The construction of the Shuanghe Arch Dam lasted from February 6, 1991 to December 5, 1992. Six vertical perforative cracks occurred on the downstream face of the arch dam soon after mid-December 1992, when the reservoir had not yet been put into operation. Cracks originated in the middle of the dam's height. Two of them had developed through the crest and four had propagated toward the foundation of the arch dam by January 1993. The sum length of the downstream face cracks was greater than 184 m. The average width of the cracks was about 1.5 mm, with a maximum of 8.0 mm. The longest crack, 2.7–3.0 m, developed on the right-hand side of the arch crown. The cracking region covered a total area of almost 900 m^2. Figure 2 shows the specific positions of the cracks and the pouring layers of the dam. Various calculation parameters are shown in Tables 2 through 6. Due to the space limitation, readers can refer to the parameters of water temperature variation in Li and Wang (2002).

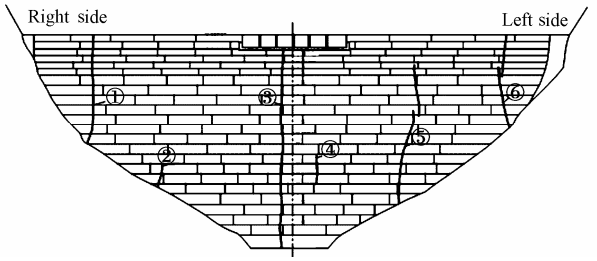

Figure 2 Pouring layers and cracks of Shuanghe Arch Dam

Table 2 Thermal properties of concrete and base foundation

Dam structure	Specific heat (kJ/(kg·℃))	Thermal diffusivity (m^2/h)	Thermal expansion coefficient (10^{-6}/℃)	Adiabatic temperature rise (℃)
Foundation		0.083 0	8.0	
Dam body	0.96	0.002 8	8.0	$\theta = 59.31t/(2.33+t)$

Note: t is the time.

Table 3 Mechanical parameters of concrete

Compressive strength (MPa)	Tensile strength (MPa)	Elastic modulus (GPa)	Ultimate tension (10^{-4})	Bulk density (kg/m^3)	Poisson ratio
13.5	0.9	14.0	0.9	2 400	0.18

The formula for the elastic modulus of concrete over time is

$$E(t) = E_0(1 - e^{-vt}) \tag{13}$$

in which $E(t)$ is the elastic modulus of concrete at a certain time, E_0 is the ultimate elastic modulus, t is the time and v is a coefficient with a value of 0.1.

The creep degree of the concrete is as follows:

$$C(t,\tau) = C_1(\tau)[1 - e^{-k_1(t-\tau)}] + C_2(\tau)[1 - e^{-k_2(t-\tau)}] \tag{14}$$

where $C_1(\tau) = C_1 + D_1/\tau$, $C_2(\tau) = C_2 + D_2/\tau$, τ is the age of concrete, and t is the time .

All the coefficients in the creep expression are shown in Table 4.

Table 4 Coefficients of creep expression

Coefficients	C_1	C_2	D_1	D_2	k_1	k_2
Value	11	280	8	28	0.25	0.008

Table 5 Statistics of meteorological factors of dam area (1957–1986)

Month	Airtemperature (℃)	Sunlight (h)	Wind speed (m/s)	Month	Airtemperature (℃)	Sunlight (h)	Wind speed (m/s)
1	5.8	36.6	1.1	7	27.6	204.4	1.2
2	7.6	40.1	1.3	8	27.5	222.2	1.2
3	12.2	80.1	1.4	9	22.8	121.5	1.3
4	17.2	111.5	1.5	10	17.5	49.7	1.1
5	20.9	110.7	1.4	11	12.4	79.5	1.1
6	24.0	129.4	1.3	12	7.7	35.4	1.0

Table 6 Placing temperature of concrete and measured data of air temperature

Initial elevation (m)	Ending elevation (m)	Initial time	Ending time	Thickness (m)	Placing temperature (℃)	Maximum temperature rise (℃)	Average air temperature (℃)	Maximum air temperature (℃)	Minimum air temperature (℃)
487.7	491.7	1991-02-06	1991-02-09	4.00	7.09	29.72	7.5	13.6	2.1
491.7	494.7	1991-03-16	1991-03-22	3.00	11.54	31.51	14.1	21.7	7.6
494.7	497.7	1991-03-25	1991-04-02	3.00	12.85	32.82	13.1	19.7	8.6
497.7	500.7	1991-04-06	1991-04-29	3.00	13.40	33.37	17.2	27.4	8.8
500.7	504.0	1991-04-12	1991-04-30	3.30	14.76	33.34	16.7	24.8	10.4
504.0	507.0	1991-04-26	1991-05-07	3.00	14.20	38.05	15.8	23.5	11.6
507.0	510.0	1991-10-30	1991-11-05	3.00	16.40	27.16	15.9	22.7	9.1
510.0	513.0	1991-11-10	1991-11-24	3.00	16.01	26.77	11.0	14.9	6.3
513.0	516.0	1991-11-21	1991-12-02	3.00	13.50	24.26	10.3	15.4	4.2
516.0	519.0	1991-12-05	1991-12-12	3.00	11.60	22.36	10.0	15.7	5.8
519.0	522.0	1991-12-17	1992-01-02	3.00	10.40	21.16	6.6	11.4	0.6
522.0	525.0	1992-01-02	1992-01-11	3.00	9.60	20.36	5.2	10.9	−0.9
525.0	528.0	1992-01-10	1992-01-19	3.00	7.57	22.18	5.4	11.6	−1.4
528.0	531.0	1992-03-11	1992-03-19	3.00	13.63	23.62	10.4	17.6	4.1
531.0	534.0	1992-03.22	1992-03-31	3.00	13.85	23.84	10.8	20.0	5.9
534.0	537.0	1992-04-05	1992-04-17	3.00	13.90	23.89	16.2	27.1	12.0
537.0	540.0	1992-04-19	1992-04-26	3.00	14.20	24.19	19.6	29.0	14.1
540.0	542.0	1992-04-29	1992-05-08	2.00	14.50	24.49	23.4	33.8	18.4
542.0	544.0	1992-05-09	1992-05-12	2.00	14.70	24.69	18.0	24.5	15.0
544.0	546.0	1992-10-15	1992-10-25	2.00	16.26	27.10	15.7	25.6	11.8
546.0	548.0	1992-10-27	1992-11-09	2.00	16.01	26.77	14.4	23.2	2.7
548.0	550.1	1992-11-12	1992-11-18	2.10	13.50	23.52	11.0	21.4	5.6
550.1	552.3	1992-11-21	1992-11-28	2.16	11.60	21.30	10.3	18.5	4.0

3.2 Simulation analysis method with consideration of construction process

The Shuanghe Arch Dam is a thin arch dam. Research shows that the temperature load is the main load on the dam, and it changes greatly over a year. Due to the dam's lack of a transverse joint, the thermal stress accumulating in the process of construction cannot be released. Moreover, temperature control was generally not studied during the dam's design period and the valid temperature control measures were not implemented during the construction period. Thus, the dam body cracked to different degrees in the course of the construction, and the cracks propagated after the reservoir was impounded. Therefore, the temperature changes during the construction period, the temperature load, the temperature

field and the stress field from the construction period to the operation period need to be analyzed in order to understand the development of the cracks in the dam.

In this study, the calculation program FEMHmadrid, developed by Pastor et al. (1997), was used for the simulation of the temperature field and stress field of the dam. The program considered almost all of the contributing factors of the temperature field and stress field of concrete, including the construction process of the arch dam and all kinds of temperature boundary conditions, such as air temperature, water temperature, solar radiation, wind speed, multiple temperature control measures, concrete creep, and autogenous volume deformation. In addition, this program has a large element library and several large equation solvers. The mixed finite element method, presented in this paper, was added to FEMHmadrid as a module.

During the pouring period, the shape of the dam was changing incessantly. According to the construction schedule, the calculation mesh was divided into different layers. At the beginning of calculation, all of the layers were locked. When a layer was poured, it was unlocked and included in the calculation. The self-weight load, the temperature load and the water pressure load of this layer were applied at the same time. In this way, the simulation analysis of the temperature field, stress field and cracking process of the arch dam from construction to operation was realized (Zhou et al. 2005).

3.3 Calculation schemes and finite element mesh

3.3.1 Calculation schemes

In order to prove the validity and accuracy of this method and to study the degree of the effect of thermal stress on arch dam cracks, three schemes were designed as follows:

Scheme I: the temperature field and stress field of the Shuanghe Arch Dam from the construction period to operation period were simulated without considering dam cracking.

Scheme II: according to the actual measured positions and number of the cracks, six contact surfaces of pair nodes were located in the FEM model of the dam. Figure 3 shows the positions of these six contact surfaces. The method presented in this paper was applied to simulation of the nonlinear cracking process.

Scheme III: apart from the contact surfaces located in scheme II, another seven contact surfaces of pair nodes were set in the positions where the cracks did not actually exist. The total number was 13, as shown in Figure 4.

3.3.2 Finite element mesh

Using GID software, the dam body according to scheme I was generated with 3D hexahedron elements and the dam foundation was generated with 3D tetrahedron elements. The finite element mesh, which included 6 609 nodes and 12 447 elements, is shown in Figure 5. Based on the mesh of scheme I, six contact surfaces of pair nodes were located in actual measured positions of the cracks in the mesh of scheme II, which included 7053 nodes and 12 791 elements. Scheme III had more contact surfaces of pair nodes, 7608 nodes and 13209 elements. The tensile strength of the contact surfaces in schemes II and III was 0.9 MPa. At the interface

between the dam body and the foundation, the compatible displacement method for a locally incompatible mesh was employed to retain the continuity of the temperature field and displacement field (Li et al. 2003).

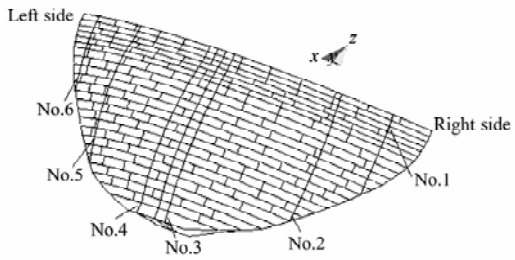

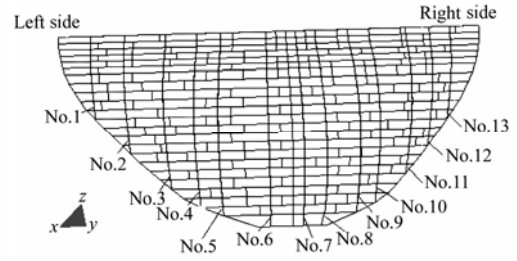

Figure 3 Position of contact surfaces in scheme II **Figure 4** Position of contact surfaces in scheme III

The calculation model approximately simulated the concreting processes of layered pouring, part by part pouring and sequence placement of the Shuanghe Arch Dam. The height of the concrete layer was 2–4 m. The concrete layer was poured twice at a single elevation. The FEM model of the dam was divided into 252 layers. When the air temperature was higher than 16.9℃, the indentation remained in the crown for concrete shrinkage. When the air temperature was lower than 16.9℃, the indentation was poured. The simulation period lasted from February 6, 1991 to November 1, 2001, 3967 days in total. The period from the 907th day to the 922nd day after pouring was a water storage period.

3.4 Comparison of stress of three schemes

Due to the space limitation, the temperature field results are not given in this paper. The maximum stress of all three schemes occurred on the 702nd day after pouring began. The distribution of the first principal stress on the downstream face in all three schemes on the 702nd day and 922nd day after pouring began is shown in Figures 6 through 8. In scheme I, the maximum first principal stress on the downstream face before impounding was 1291.6 kPa. After impounding was finished, the tensile stress became smaller, the maximum value was 919.22 kPa, and the maximum tensile stress before and after impounding occurred at the same position. In scheme II, the maximum first principal stress on the downstream face was 1 199.3 kPa before impounding and 853.09 kPa after impounding. The position where the maximum first principal stress occurred was consistent with that in scheme I, although the value was a bit smaller, but at the left and right abutment before water impounding and the 1/4 left and right arch on the upstream face after impounding, the tensile stress was relatively large. The latter in

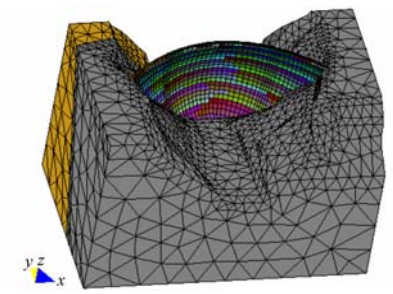

Figure 5 Finite element mesh for arch dam

particular possibly caused the cracks between the upstream dam face and the foundation, so it should be considered in reinforcement design. The maximum first principal stress on the downstream face in scheme III was 1198.7 kPa before impounding and 820.23 kPa after impounding. The position was consistent with that in scheme II.

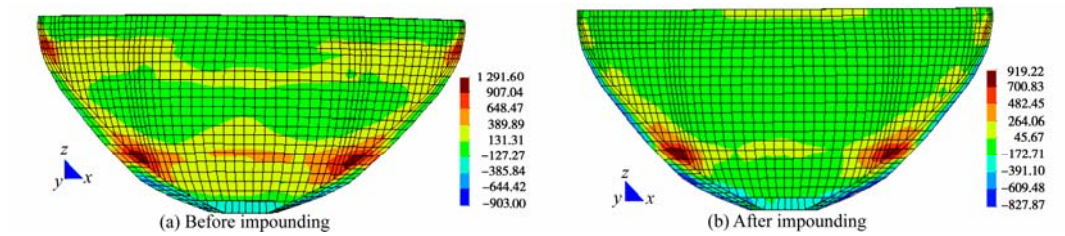

Figure 6 First principal stress on downstream face in scheme I (unit: kPa)

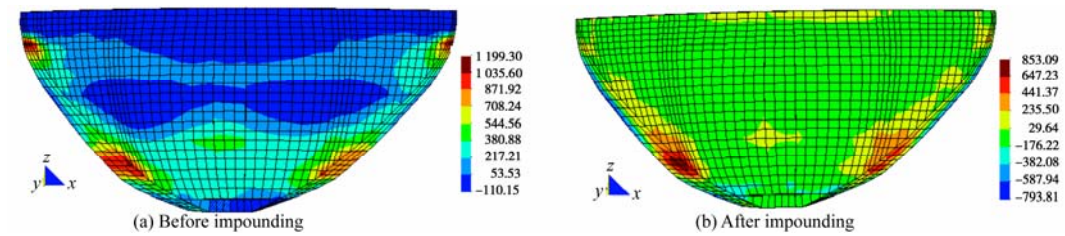

Figure 7 First principal stress on downstream face in scheme II (unit: kPa)

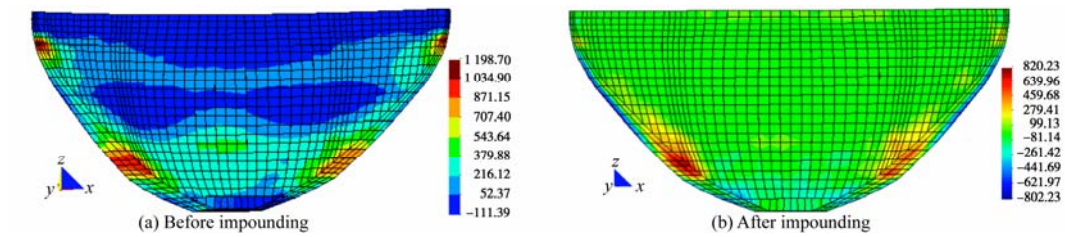

Figure 8 First principal stress on downstream face in scheme III (unit: kPa)

3.5 Discussion of cracking simulation results of scheme Ⅱ

The opening areas shown in Figures 9 and 10 agree with the measured data. Figure 11 shows the opening value of a typical pair of nodes on six contact surfaces over time. The positions of the typical nodes are shown in Figure 10. The opening values of all contact surfaces were largest on the 702nd day after pouring, and the maximal value was 5.136mm. Impounding began on the 902nd day after pouring and lasted 20 days. The results show that water pressure can limit the growth of cracks, especially downstream face cracks, and the length of the upstream face cracks decreased after impounding. The cracking positions, cracking areas and cracking time calculated with this method basically match up with the measured data. However, besides the temperature load, a main influencing factor, there were other factors affecting the cracking of the Shuanghe Arch Dam. For example, the material of the foundation is extremely heterogeneous, so the simulated opening value was not equal to what was actually measured, but the general tendency was almost the same.

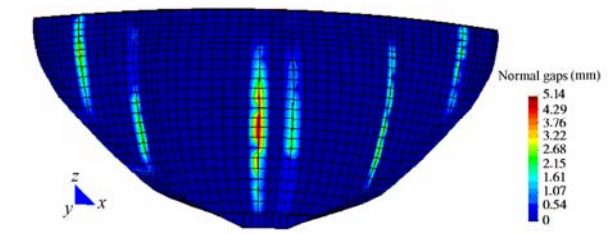

Figure 9 Opening value of downstream face on the 702nd day after pouring

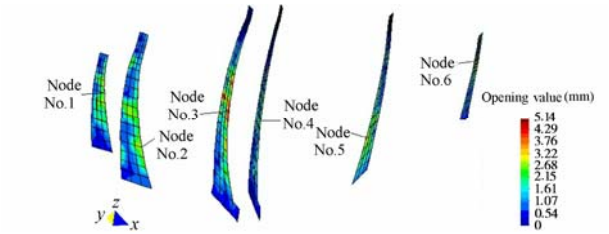

Figure 10 Positions of typical nodes on contact surfaces on the 702nd day after pouring

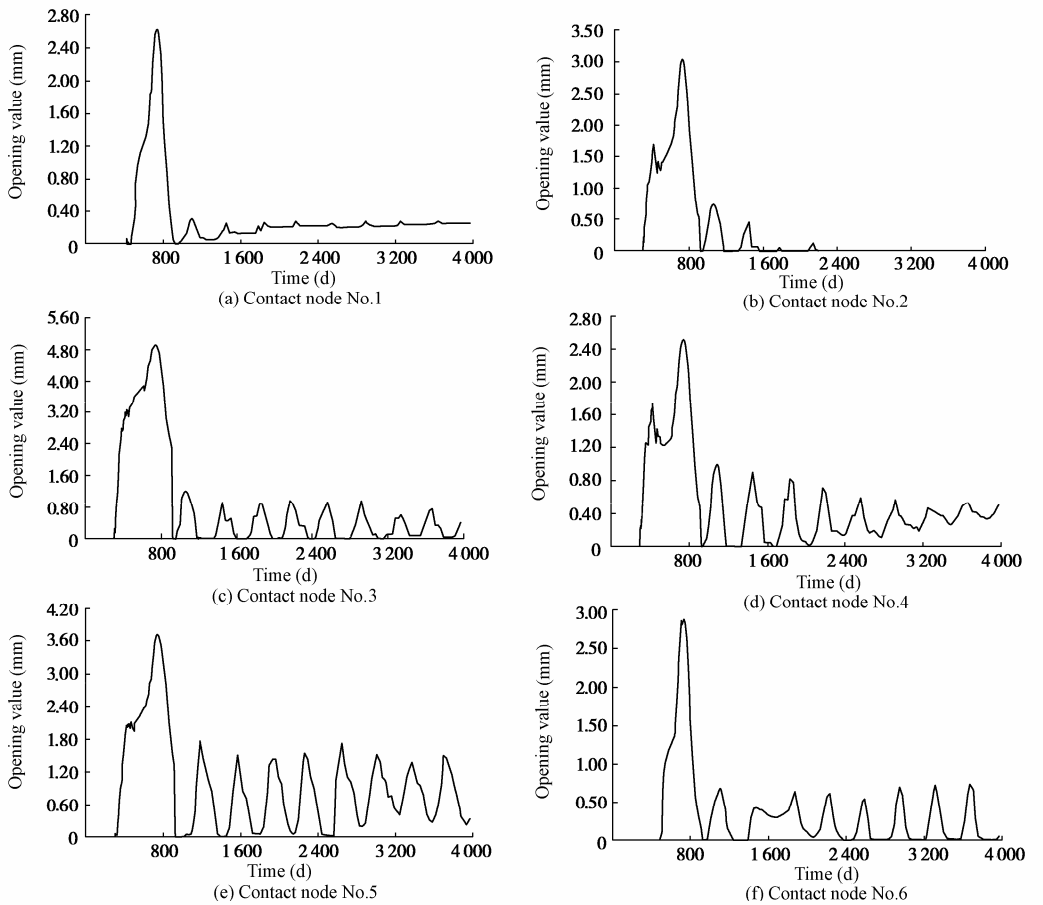

Figure 11 Opening value of typical contact nodes over time

3.6 Comparison of cracking simulation results of scheme Ⅱ and scheme Ⅲ

Figure 12 shows the cracking of six contact surfaces of pair nodes on which the opening value was greater than 2.5 mm in scheme II. Figure 13 shows the cracking pair nodes on 13 contact surfaces on which the opening value was greater than 1.7 mm in scheme III. The contact surfaces of numbers 1, 3, 6, 7, 10 and 13 in scheme III correspond to the contact surfaces of numbers 1 through 6 in scheme II. The maximum opening value was 4.82 mm in scheme III. Comparison of the results of the two schemes shows that the cracking numbers and cracking position of the contact surface in scheme III were similar to those of scheme II. Only the opening value in scheme III was relatively smaller. The additional seven contact surfaces of pair nodes in scheme III were not cracked.

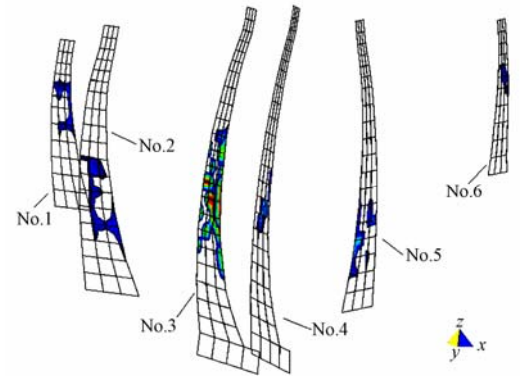

Figure 12 Opening area of six contact surfaces on the 702nd day after pouring in scheme II

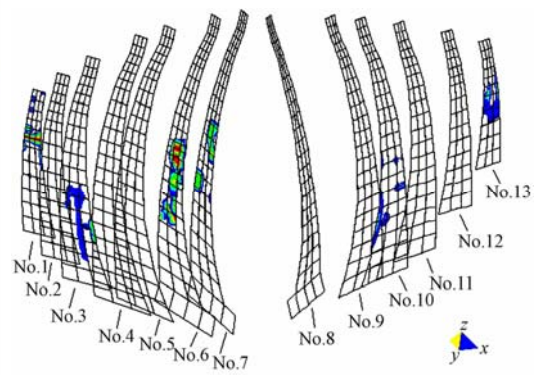

Figure 13 Opening area of thirteen contact surfaces on the 702nd day after pouring in scheme III

4 Conclusions

(1) In the FEM model, the friction-contact mixed finite element method was used to simulate the cracking process. When the contact surfaces of pair nodes were located at the sites of possible cracking of the dam, the numerical results of the nonlinear cracking showed that the cracking positions, cracking areas and cracking time calculated by this method basically match up with the actual measured data. When the contact surfaces of pair nodes were located in the non-cracking area, the numerical results demonstrated that there wasn't any crack occurring. The method presented in this paper converges relatively well. Generally, only five steps of iterations are necessary to obtain the correct result. The computational efficiency of this method is seven times that of the full freedom iterative solution method, and three times that of the flexibility method.

(2) The stress results show that the existence or absence of dam cracking has little effect on the stress distribution of the dam, but the tensile stress value that considers dam cracking is smaller than that without consideration of cracking. This is because the tensile stress is

partially released by the opening of cracks.

(3) Under the circumstance of a given crack location and ordinary cracking track, mesh distribution is relatively easy to draw, and the method described in this paper is efficient. However, if the crack location and depth are unknown, it is hard to plot the appropriate mesh. More research must be done to expand the results presented in this paper.

References

Francavilla, A., and Zienkiewicz, O. C. 1975. A note on numerical computation of elastic contact problems. *International Journal for Numerical Methods in Engineering*, 9(4), 913–924.

Haug, D., and Saxce, G. 1980. Frictionless contact of elastic bodies by finite element method and mathematical programming technique. *Computers Structures*, 11(1-2), 55–67.

Kikuhci, N. 1982. A smoothing technique for reduced integration penalty methods in contact problems. *International Journal for Numerical Methods in Engineering*, 18(3), 343–350.

Lei, X. Y., Swobode, G., and Du, Q. H. 1994. Theory and application of contact-friction interface element. *Chinese Journal of Geotechnical Engineering*, 16(3), 23–32. (in Chinese)

Li, T. C., and Wang, R. K. 2002. *Simulation Analysis of Dangerous Shuanghe Arch Dam and Reinforcement Project Research*. Nanjing: Hohai University. (in Chinese)

Li, T. C., Li, M., and Wen, Z. W. 2003. Application of locally incompatible meshes to stress analysis of high arch dams. *Journal of Hohai University* (*Natural Sciences*), 31(1), 42–45. (in Chinese)

Pastor, M., Li, T. C., and Fernández Merodo, J. A. 1997. Stabilized finite elements for harmonic soil dynamics problems near the undrained-incompressible limit. *Soil Dynamics and Earthquake Engineering*, 16(3), 161–171.

Peric, D., and Owen, D. R. J. 1992. Computational model for 3D contact problems with friction based on the penalty method. *International Journal for Numerical Methods in Engineering*, 35(6), 1289–1309.

Shao, W., Jin, F., and Wang, G. L. 1999. Nonlinear thin-layer element for modeling interface. *Journal of TsingHua University* (*Science and Technology*), 39(2), 34–38. (in Chinese)

Simo, J. C., Wrigger, P., and Tayor, R. L. 1985. A perturbed lagrangian formulation for the finite element solution of contact problems. *Computer Methods in Applied Mechanics and Engineering*, 50(2), 163–180.

Wang, S. L., Deng, J. H., and Ge, X. R. 1998. Application of augmented Lagrangian method in frictional contact problem. *Chinese Journal of Geotechnical Engineering*, 20(5), 64–67. (in Chinese)

Yang, L.Q. 2003. *Cracking Analysis and Safety Evaluation for High Arch Dam*. Ph.D. Thesis. Tianjin: Tianjin University. (in Chinese)

Zhang, G. X., Yang, B., Shen, X. P., Zhu, B. F., and Zhao, Q. 2004. Nonlinear analysis of cracks in gentle volume expansive concrete arch dam. *Journal of Hydroelectric Engineering*, 23(3), 51–55. (in Chinese)

Zhao, L. H., and Li, T. C., and Liu, Z. W. 2006. Mixed finite element method for contact problems with friction and initial gaps. *Chinese Journal of Geotechnical Engineering*, 28(11), 2015–2018. (in Chinese)

Zhao, L. H., and Li, T. C., and Liu, Z. W. 2007. The dynamic contact model of nonlinear seismic response of high arch dams with contraction joints. *Journal of Hydroelectric Engineering*, 26(4), 92–95. (in Chinese)

Zhou, W., Chang, X. L., and Liu, X. H. 2005. Study of RCC gravity dam parting design with considering temperature stress influence. *Journal of Hydroelectric Engineering*, 24(6), 25–29. (in Chinese)